Electric-field-dependent phase volume fractions and enhanced piezoelectricity near the polymorphic phase boundary of (K_{0.5}Na_{0.5})_{1-x}Li_{x}NbO_{3} textured ceramics

Wenwei Ge, Jiefang Li, D. Viehland, Yunfei Chang, and Gary L. Messing

Phys. Rev. B **83**, 224110 — Published 24 June 2011

DOI: 10.1103/PhysRevB.83.224110

Electric field dependent phase volume fractions and enhanced piezoelectricity near the polymorphic phase boundary of $(K_{0.5}Na_{0.5})_{1-x}Li_xNbO_3$ textured ceramics

Wenwei Ge,[a] Jiefang Li, and D. Viehland

Department of Materials Science and Engineering, Virginia Tech, Blacksburg, Virginia 24061

Yunfei Chang, and Gary L. Messing

Department of Materials Science and Engineering, Pennsylvania State University, University Park, Pennsylvania 16802

Abstract

The structure and ferroelectric/piezoelectric properties of <001>-textured $(K_{0.5}Na_{0.5})_{0.98}Li_{0.02}NbO_3$ ceramics were investigated as a function of temperature and dc bias (E). X-ray diffraction revealed an orthorhombic (O)→tetragonal (T) polymorphic phase boundary (PPB). Phase coexistence was found near the PPB over a 30^{o}C temperature range, where the relative phase volume fractions changed with temperature. Furthermore, increasing E applied along the <001>-texture direction resulted in a notable increase in the volume fraction of the T phase at the expense of the O phase, effectively shifting the O→T boundary to lower temperature. An enhancement in the piezoelectric properties was found to accompany this increase in the T volume fraction.

[a] Electronic mail: wenweige@vt.edu

I. Introduction

The high electromechanical properties of $Pb(Zr_xTi_{1-x})O_3$ (or PZT) ceramics for compositions near the morphotropic phase boundary (MPB) [1] form the basis of piezoelectric actuators, transducers and sensors. However, these lead-based materials pose environmental concerns, due to the volatility and toxicity of PbO during material preparation. Thus, lead-free piezoelectric materials have attracted attention in recent years [2].

$KNbO_3$ and $NaNbO_3$ form a complete solid solution of $K_{1-x}Na_xNbO_3$ (KNN) over the entire range of $0<x<1$ [3]. KNN undergoes a structural phase transformation sequence on cooling of paraelectric Cubic (C) $\xrightarrow{\sim 415^\circ C}$ ferroelectric Tetragonal (T) $\xrightarrow{\sim 210^\circ C}$ ferroelectric Orthorhombic (O) $\xrightarrow{\sim -150^\circ C}$ ferroelectric Rhombohedral (R) [1, 3, 4]. The T→O boundary is known as the polymorphic phase boundary (PPB) to designate its difference with the MPB. The PPB of KNN solid solutions is nearly independent of x, remaining unchanged in temperature for $0<x<1$ [1, 3, 5]. This is in distinct contrast to the MPB for PZT, which is nearly independent of temperature and fixed near $x=0.5$ [1].

Accordingly, the piezoelectric properties of KNN are not independent of temperature like that of MPB compositions of PZT [1]. A broad maximum in the planar coupling coefficient k_p centered at $x=0.5$ is known for $K_{1-x}Na_xNbO_3$ ceramics, prepared either by conventional solid-state reaction [6] or hot pressing [4, 7] methods. More recently, an enhanced longitudinal piezoelectric coefficient of d_{33}=410 pC/N was reported for <001>-textured $(K_{0.44}Na_{0.52}Li_{0.04})(Nb_{0.86}Ta_{0.10}Sb_{0.04})O_3$ ceramics [8].

This value is close to that of "soft" PZT ceramics [1]. This report has triggered an extensive search to further improve d_{33} of the KNN system by use of various substituents: examples include $LiNbO_3$ (LN), $LiSbO_3$ (LS), $LiTaO_3$ (LT), $BaTiO_3$, $CaTiO_3$, and $SrTiO_3$ [9-20]. Indeed, the room temperature piezoelectric properties of KNN have been enhanced by doping with LN, LS and LT [9, 11, 14]. Temperature dependent piezoelectric measurements for KNN-based materials revealed that maximum piezoelectric properties existed at a narrow temperature range near the T→O boundary and the enhancements in d_{33} of KNN-based solid solutions by compositional modifications have been shown to result from a shifting of the PPB to lower temperatures: from ~210 °C for pure KNN, to near room temperature for those with the highest d_{33} values [12, 14].

These facts indicate the mechanism of enhanced piezoelectricity near the PPB is quite different with that of near the MPB. The mechanism of high piezoelectricity in Pb-based MPB compositions is believed to be due to low-symmetry structurally bridging phases, where polarization rotation may occur in a plane [21-27]. However, the mechanism of enhanced piezoelectricity near the PPB of KNN-based solutions is not yet clear. Ahn et al [28] reported that high piezoelectric properties were observed when the tetragonal phase volume fraction was ~70% in Li-modified KNN ceramics. However, how the electric field (E) effects the T and O phases near the PPB boundary has not yet been reported. Such investigations would yield new insights to understanding the mechanism of enhanced piezoelectricity near the PPB.

Compared to conventional randomly oriented KNN ceramics, <001>-textured

KNN ceramics exhibited much better piezoelectric properties [29]. Here, we report an investigation of the E-field dependent phase stability of <001>-textured $(K_{0.5}Na_{0.5})_{0.98}Li_{0.02}NbO_3$ (or 2at% Li:KNN) ceramics. Our findings demonstrate the presence of a two-phase T and O field near the PPB, where the volume fractions of the phases change with temperature and electric field. An E-field applied along <001> increases the volume fraction of the T phase, effectively decreasing the T→O boundary temperature. An enhancement in d_{33} was found to accompany the increase of the T volume fraction under E. These findings demonstrate a notably different phase transformation mechanism, and resultant enhanced properties, in materials with a PPB in contrast to those with a MPB.

II. Experimental procedure

<001>-textured 2at%Li:KNN ceramics were prepared by a templated grain growth (TGG) technique developed by Messing et al[29-32]. The texture fraction or Lotgering factor of 2at%Li:KNN textured samples was estimated to be 98%[29]. Samples were cut into 5x5x0.5 mm^3 plates, and subsequently electroded on both surfaces with gold. Temperature dependent dielectric constant measurements were performed using a LCR meter (HP 4284A) under dc electric fields of E=0, 2, 4, 6, 8, 10 and 12 kV/cm. Polarization hysteresis loops (P-E) and unipolar strain vs E-field curves (ε-E) were measured in the temperature range of 30 to 150^{o}C at a frequency of 1Hz using a modified Sawyer-Tower circuit and a linear variable differential transducer (LVDT) driven by a lock-in amplifier (Stanford Research, SR850).

Piezoelectric d_{33} constants were measured using a quasistatic Berlincourt d_{33} meter. Temperature dependent X-ray line scans were taken using a Philips MPD high-resolution diffractometer under E-fields of 0, 6 and 12 kV/cm in the temperature range from 30 to 140^{o}C on cooling. The x-ray wavelength was that of Cu K_{α} =1.5406 Å, and the x-ray generator was operated at 45 kV and 40 mA.

III. Results and discussions

(A) Property studies

Figure 1(a) shows the temperature dependent 1 kHz dielectric constant ε_r and loss factor tanδ for KNN-2%LN taken on heating over the temperature range of 25 to 580^{o}C. Two dielectric peaks can be seen. A sharp dielectric maximum was found near 425^{o}C, corresponding to the Curie temperature T_C. A second broader dielectric peak was observed near 143^{o}C, corresponding to the O→T boundary or PPB. A thermal hysteresis of ~15^{o}C was apparent between heating and cooling measurements near this boundary, as can be seen in the insert of Fig.1. This hysteresis indicates the presence of a notable transformation strain at the O→T boundary. Compared to pure KNN (T_C~415^{o}C and T_{O-T}~210^{o}C) [3], the value of T_C was slightly increased, whereas that of T_{O-T} was decreased by addition of 2% LN. These trends for textured KNN-2%LN are consistent with ones for conventional KNN-LN ceramics [16].

Figure 1(b) shows the P-E hysteresis loops at various temperatures, which were taken under a maximum ac electric field of E_{ac}= 80 kV/cm on heating. At 30^{o}C, the coercive electric field and the remnant polarization were E_c=21 kV/cm and P_r=15.5

μC/cm^2. With increasing temperature, P_r first increased and then decreased, reaching a peak value of P_r=19 μC/cm^2 at 130^{o}C (see Fig.1d) near the PPB. Figure 1(c) shows the unipolar ε-E curves under E_{ac}=40 kV/cm. At 30^{o}C, the maximum electrically induced strain was 0.09%, whereas at 120^{o}C it increased to 0.16% and slightly decreased to 0.12% at 150^{o}C.

Next, we calculated the large-amplitude effective d_{33} coefficient ($\boldsymbol{\varepsilon_3 = d^*_{33} \cdot E_3}$) from the slope of ε-E [33]. The values of d^*_{33} over a temperature range of 30 to 150^{o}C are shown in Fig.1(d). At 30^{o}C, d^*_{33} was about 200 pC/N. In addition, after the unipolar ε-E measurements were finished, the d_{33} value was also directly measured at room temperature using a Berlincount meter and found to be about 190 pC/N, in agreement with the large signal value. With increasing temperature, the values of d^*_{33} increased, reaching values as high as 400 pC/N, at temperatures near the PPB. The data in Fig.1(d) demonstrate that the induced polarization and piezoelectric constants are sharply peaked over a modest temperature range around the PPB: d^*_{33} increased by 100%, while P_r only increased by 20%. This means the enhancement was not simply due to increased polarization with increasing temperature. Chang et al [29] previously found that low field piezoelectric properties, such as electromechanical coupling factors (k_p and k_{31}) and piezoelectric d_{31} constants of 2at%Li:KNN textured ceramics were enhanced near the PPB. Clearly, the enhanced electromechanical properties are related to structural and/or domain changes in the vicinity of the PPB.

Figure 2 shows the dc-bias dependent 1 kHz dielectric data taken on cooling. With increasing bias (E), we can make three observations. First, the dielectric constant

in the T phase was notably decreased with increasing E, whereas that in the O phase was nearly unchanged (see Fig.2a). To better illustrate the dramatic dc-bias dependent dielectric constant, we define the tunability of ε_r as $[\varepsilon_r(E)-\varepsilon_r(0)]\times 100\%/\varepsilon_r(0)$, where $\varepsilon_r(0)$ and $\varepsilon_r(E)$ are the dielectric constant under zero dc bias and under a bias of E, respectively. The tunability of ε_r at 180^{o}C (in the T phase field) and at 25^{o}C (in the O phase field) are shown as a function of E in Fig.2(c). In the T phase field, ε_r can be seen to decrease by about 60% in a near-linear manner with increasing bias for $0<E<12$kV/cm. Second, the dielectric loss factor tanδ decreased with increasing E in both the T and O phase fields. This demonstrates that the imaginary dielectric constant ($\varepsilon''=\varepsilon_r\cdot\tan\delta$) is notably dependent on E in the O phase field, even though ε_r is nearly independent of E. The energy stored in the dielectric is unaltered by bias in the O phase, yet that dissipated is decreased. Third, for $E\geq 4$ kV/cm, the secondary dielectric peaks corresponding to the T→O transition of the PPB became increasingly sharp with increasing E, as indicated by the arrow. In addition, the T→O boundary modestly shifted to lower temperatures with increasing E. We summarize this shift of the T→O PPB (taken on cooling) in Figure 2(d), which shows that the PPB was decreased by about 20^{o}C with increasing bias for $0<E<12$ kV/cm. Furthermore, this figure shows that the thermal hysteresis given in the insert of Fig.1(a) was nearly independent of E.

(B) Structural studies

To better understand the influence of E on the dielectric properties, we performed temperature dependent structural investigations by XRD. Studies were done about the {200} zones under various dc biases, beginning from high temperatures in the T phase

and cooling into the O phase to room temperature. In Fig.3(a), two sharp diffraction peaks can be seen at 140°C, which correspond to the $(002)_T$ and $(200)_T$ reflections of the T phase. With decreasing temperature to 112°C, a third small peak appeared at slightly higher 2θ values than the $(200)_T$, demonstrating the formation of a small volume fraction of O phase. With decrease of temperature to 108°C, the intensity of the $(200)_O$ peak increased, while the intensity of $(200)_T$ decreased. In addition, a fourth $(022)_O$ broad peak began to form between $(002)_T$ and $(200)_T$. With further decrease of temperature, the intensity of the $(200)_O$ and $(022)_O$ peaks increased, whereas the $(002)_T$ and $(200)_T$ peaks decreased. At 84°C, the $(002)_T$ and $(200)_T$ peaks could not be detected.

These structural results for the zero-field-cooled (ZFC) state reveal (i) a single T phase field at >112°C; (ii) a T+O two phase field for temperatures between 112°C and 84°C, where the volume fraction of the O phase increases at the expense of the T with decreasing temperature; and (iii) a single O phase field at <84°C. The T→O transition of KNN is not required by symmetry to be 1st order, as there exists a group-subgroup relationship between the point group symmetries. However, phase coexistence is well known near boundaries between phases undergoing a 1st order transition. It is relevant to note that two phase coexistence about the MPB in Pb-based perovskites, even though originally believed responsible for enhanced piezoelectricity [1], is not supported by structural evidence: rather, low symmetry structurally bridging monoclinic phases exist [22]. Our findings clearly demonstrate phase coexistence about the PPB in 2at% Li:KNN, and indicate its probable influence on enhanced

piezoelectric properties.

We investigated the structure of 2at% Li:KNN under field-cooled (FC) condition by XRD. A notable change in the 2θ line scans was apparent in the FC state, relative to the ZFC. Under E=6kV/cm (data not shown), the $(200)_O$ and $(022)_O$ peaks [34] began to become apparent on cooling between 112°C and 108°C, similar to the ZFC condition but were much weaker in intensity than for ZFC. Under E=12kV/cm, $(200)_O$ and $(022)_O$ peaks were not observed at 108°C in Fig.3b. With decrease of temperature to 104°C, a broad $(022)_O$ peak became apparent; however, the $(200)_O$ peak was too low in intensity to be detected. On cooling to 84°C, the $(002)_T$ and $(200)_T$ peaks completely disappeared. These results demonstrate that the stability range of the T phase field is expanded by application of E//<001>-texture, consistent with the shift of the PPB to lower temperatures with E in the dielectric constant, as shown in Fig.2(d).

Next, we calculated the relative volume fractions of the T (V_T) and O (V_O) phases as

$$V_T=[I_{(002)_T}+I_{(200)_T}]/[I_{(002)_T}+I_{(200)_T}+I_{(022)_O}+I_{(200)_O}], \qquad (1)$$

and

$$V_O=[I_{(022)_O}+I_{(200)_O}]/[I_{(002)_T}+I_{(200)_T}+I_{(022)_O}+I_{(200)_O}]; \qquad (2)$$

where $I_{(002)T}$, $I_{(200)T}$, $I_{(002)O}$, $I_{(200)O}$ are the integrated intensities of the tetragonal (002) and (200) peaks, and orthorhombic (022) and (200) peaks, respectively. The temperature dependences of V_T and V_O are given in the Fig.3(c) under E=0, 6, and 12kV/cm. Inspection of this figure reveals that V_T and V_O are dependent on bias in the

temperature range of the two phase coexistence. A dc bias applied along the <001>-texture favored the T phase over the O. For example, at 105^{o}C, the volume fraction of the T phase increased from about 0.7 to 0.9 by E=12kV/cm. Clearly, changes in relative phase stability occur near the PPB under bias, and these changes correlate to an enhancement in the piezoelectric constant, as will be discussed in section III (D).

(C) Domain configurations

Figure 4 shows schematics of the possible domain configurations in the T and O phases, in the ZFC (left column) and FC (right column) conditions. In the T phase, the domain orientations must be either parallel or perpendicular to the <001>–texture direction. We first illustrate the simplest case of the ZFC as shown in Fig.4(a): white denotes c-domain regions, and gray a-domain regions. The c- and a-domain orientations contribute to the $(002)_T$ and $(200)_T$ reflections, respectively. Thus, the volume fraction of tetragonal c-domains can be estimated as $I_{(002)T}/[I_{(002)T}+I_{(200)T}]$. On transforming to the O phase, the tetragonal c-domains change into four equivalent orthorhombic ones: which are $[0\bar{1}1]_{cub}$, $[\bar{1}01]_{cub}$, $[011]_{cub}$ and $[101]_{cub}$, as shown in Fig.4(b) with thick arrows. These O type I domains give contributions to the $(022)_O$ reflections. Furthermore, at the transformation, the tetragonal a-domains change into two equivalent orthorhombic ones in the a-b plane: which are $[110]_{cub}$ and $[\bar{1}10]_{cub}$, as shown in Fig.4(b) with thin arrows. These O type II domains give contributions to the $(200)_O$ reflections. Thus, the volume fraction of O type I domains can be estimated as $I_{(022)O}/[I_{(022)O}+I_{(200)O}]$.

Finally, we calculated how the O and T domain distributions were affected by temperature and E. The ratios $I_{(002)T}/[I_{(002)T}+I_{(200)T}]$ and $I_{(022)O}/[I_{(022)O}+I_{(200)O}]$ are given as a function of temperature under E=0, 6 and 12kV/cm in both the T and O phase fields in Fig.3(d). The intensity ratios in the T+O two phase field are not shown, as their values fluctuated notably when either $I_{(002)T}$ or $I_{(022)O}$ was close to zero. In Fig.3(d), it can be seen that $I_{(002)T}/[I_{(002)T}+I_{(200)T}]$ and $I_{(022)O}/[I_{(022)O}+I_{(200)O}]$ were nearly independent of temperature in the T and O phase fields, respectively. This demonstrates that the domain distribution for both the T and O phases did not change notably with temperature. However, the intensity ratios were strongly dependent on E, as can be seen in Fig.3(d). At 140^{o}C, the value of $I_{(002)T}/[I_{(002)T}+I_{(200)T}]$ increased from 0.66 under zero bias to 0.96 under E=12 kV/cm. This shows that the volume fraction of the tetragonal c-domains increased by 30% under E=12 kV/cm, becoming nearly a single c-domain state, as schematically illustrated in Fig.4(c). Clearly, the domain distributions in the T single phase field are notably changed by E.

Thus, one can explain the large tunability of ε_r with E in the T phase field as resulting from an increase in the volume fraction of c-domains at the expense of the a-domains under E//<001>-texture. In the O phase field at 30^{o}C, the value of $I_{(022)O}/[I_{(022)O}+I_{(200)O}]$ increased from 0.88 under zero bias to 1 under E=6 kV/cm. This shows that the volume fraction of O type I domains increased by 12% at the expense of elimination of O type II, as sketched in Fig.4(d) with dashed arrows. Clearly, the dielectric constant for <001>-textured 2at% Li:KNN ceramics in the O phase field is mostly a contribution of O type I domains. It is note-worthy that these four O type I

domains are equivalent to E applied along [001]-texture, as illustrated in Fig.4(d). Accordingly, the tunability of ε_r with E in the O phase field is quite small (see Fig.2). The fact that the four O type I domains are equivalent and that ε_r is nearly independent of E in the O phase indicates that rotation of the polarization in the O type I domains (i.e., $[0\bar{1}1]_{cub}$, $[\bar{1}01]_{cub}$, $[011]_{cub}$ and $[101]_{cub}$) towards the $[001]_{cub}$ probably does not tend to occur, at least in the O single phase region.

(D) Correlation between relative phase stability and enhanced piezoelectric properties near the PPB

In crystals belonging to the tetragonal 4mm point group, the value of the longitudinal piezoelectric coefficient d_{33}^* as a function of orientation (θ) in the crystallographic coordinate system is given by [35]

$$d_{33}^*(\theta) = \cos\theta(d_{15}^T \sin^2\theta + d_{31}^T \sin^2\theta + d_{33}^T \cos^2\theta); \qquad (3)$$

where

$$d_{15}^T = \varepsilon_0 \varepsilon_{11}^T Q_{44} P_3^T \qquad (4)$$

$$d_{31}^T = 2\varepsilon_0 \varepsilon_{33}^T Q_{12} P_3^T \qquad (5)$$

$$d_{33}^T = 2\varepsilon_0 \varepsilon_{33}^T Q_{11} P_3^T . \qquad (6)$$

The angle θ describes the rotation away from the $[001]_T$ axis of the tetragonal unit cell; the various Q are electrostriction coefficients; P_3 is the spontaneous polarization; ε_o is the permittivity of vacuum; and ε_{11} and ε_{33} are the permittivities along directions perpendicular and parallel to the direction of the spontaneous polarization P_3. Generally, d_{31} is negative and smaller than either d_{15} or d_{33} in most perovskite ferroelectrics [36]. Thus, d_{33}^* is dominated by the shear d_{15}^T and longitudinal d_{33}^T

coefficients. For <001>-textured 2at% Li:KNN ceramics in the T phase field, the a- and c-domains (see Fig.4a and 4c) contribute to ε_{11}^{T} and ε_{33}^{T}, respectively. Our experimental data shows that the volume fraction of the T a-domains decreased by 30% under application of E=12 kV/cm (see Fig.3d), whereas the dielectric constant in the T phase was decreased by as much as 60% (see Fig.2a). These results suggest that the transverse permittivity ε_{11}^{T} is much higher than the longitudinal one ε_{33}^{T} in the T phase field. This means d_{15}^{T} (which is $\propto \varepsilon_{11}^{T}$ from (4), and related to the volume fraction of T a-domains) contributes more than d_{33}^{T} (which is $\propto \varepsilon_{33}^{T}$ from (6), and related to the volume fraction of the T c-domains) to the effective value of d_{33}^{*}. Both phenomenological and basic principle calculations have shown that the transverse permittivity is enhanced in the vicinity of phase transitions between two ferroelectric phases, where the polarization changes direction [36]. Thus, d_{15}^{T} will be significantly increased as the O phase is approached on cooling. Consequently, d_{33}^{*} should have a peak value near the T→O PPB boundary (see Fig.1d).

In the T phase field, the domain distributions were strongly E-field dependent and the volume fraction of the T a-domains were decreased by E (see Fig.3d). Accordingly, the contribution from d_{15}^{T} was decreased, and d_{33}^{*} in the T phase is lower than that near the PPB. In the O phase field, similar thought applies, although the situation is a little more complex [35]. When the O phase field is entered on crossing the PPB with decreasing temperature, the T a-domains change into O type II domains (see Fig.4b), which contributes to the value of ε_{11}^{O}: even though ε_{11}^{O} is larger than either ε_{22}^{O} or ε_{33}^{O}, it is significantly smaller than ε_{11}^{T}. Thus, the value of d_{33}^{*} is

decreased on entering the O phase field.

From Figure 3(c), one can see that the dependence of the phase volume fraction on E was highest when V_T≈65%-80%. For example, at 105°C, the value of V_T was increased by 28% (from about 0.7 to 0.9) under application of E=12 kV/cm. From these results combined with the above discussion, one can conclude that the contribution of the T phase to the enhancement of d_{33}^* is higher than that of the O phase near the PPB. Recently, Ahn et al. [28] reported a correlation of a higher value of d_{33} at room temperature with a higher value of V_T (~70%) for (K,Na,Li)NbO_3-$BaTiO_3$ ceramics. In Figure 3(d), one can see in the single T phase field that the volume fraction of the T a-domains was significantly decreased by E, whereas in the single O phase field the domain distribution was only slightly dependent on E. These results indicate that the optimum poling temperature for KNN-based materials by which to achieve enhanced piezoelectricity is near the PPB boundary, as reported by Du et al [37].

IV. Summary

Our findings demonstrate that O and T phases that coexisted over a 30°C range near the PPB. These two phases were distinct and individually identifiable (and thus separable) by XRD. The O and T phases in the two phase field are in thermodynamic equilibrium with each other. This is supported by the fact that the relative volume fractions of the T and O phases were dependent on temperature and electrical field: i.e., they follow a "lever-like" rule. Furthermore, changes in V_T and V_O were reversible with decrease/increase of temperature and field. Application of electric bias

along <001>-texture was found to favor the T phase, and to shift the PPB to lower temperatures. Our results indicate that the enhanced piezoelectric properties near the PPB are due to this susceptibility of volume fractions of tetragonal phase to electrical field.

Acknowledgements

This work was supported by the National Science Foundation (Materials world network) DMR-0806592 and by the Department of Energy under DE-FG02-07ER46480.

References

[1] B. Jaffe, W. R. Cook, and H. Jaffe, *Piezoelectric Ceramics* (Academic Press Inc., U. S, London and N.-Y., 1971).

[2] E. Cross, Nature **432**, 24 (2004).

[3] G. Shirane, R. Newnham, and R. Pepinsky, Phys. Rev. **96**, 581 (1954).

[4] R. E. Jaeger and L. Egerton, J Am Ceram Soc **45**, 209 (1962).

[5] L. Wu, J. L. Zhang, C. L. Wang, and J. C. Li, Journal of Applied Physics **103**, 084116 (2008).

[6] L. Egerton and D. M. Dillon, J Am Ceram Soc **42**, 438 (1959).

[7] G. H. Haertling, J Am Ceram Soc **50**, 329 (1967).

[8] Y. Saito, H. Takao, T. Tani, T. Nonoyama, K. Takatori, T. Homma, T. Nagaya, and M. Nakamura, Nature **432**, 84 (2004).

[9] Y. P. Guo, K. Kakimoto, and H. Ohsato, Appl Phys Lett **85**, 4121 (2004).

[10] E. Hollenstein, M. Davis, D. Damjanovic, and N. Setter, Appl Phys Lett **87**, 182905 (2005).

[11] G. Z. Zang, J. F. Wang, H. C. Chen, W. B. Su, C. M. Wang, P. Qi, B. Q. Ming, J. Du, and L. M. Zheng, Appl Phys Lett **88**, 212908 (2006).

[12] S. J. Zhang, R. Xia, T. R. Shrout, G. Z. Zang, and J. F. Wang, Journal of Applied Physics **100**, 104108 (2006).

[13] K. Wang and J. F. Li, Appl Phys Lett **91**, 262902 (2007).

[14] Y. Dai, X. Zhang, and G. Zhou, Appl Phys Lett **90**, 262903 (2007).

[15] D. Lin, K. W. Kwok, and H. W. L. Chan, Appl Phys Lett **91**, 143513 (2007).

[16] X. K. Niu, J. L. Zhang, L. Wu, P. Zheng, M. L. Zhao, and C. L. Wang, Solid State Communications **146**, 395 (2008).

[17] J. L. Zhang, X. J. Zong, L. Wu, Y. Gao, P. Zheng, and S. F. Shao, Appl Phys Lett **95**, 022909 (2009).

[18] H.-Y. Park, C.-W. Ahn, H.-C. Song, J.-H. Lee, S. Nahm, K. Uchino, H.-G. Lee, and H.-J. Lee, Appl Phys Lett **89**, 062906 (2006).

[19] R. P. Wang, R. J. Xie, K. Hanada, K. Matsusaki, H. Bando, T. Sekiya, and M. Itoh, Ferroelectrics **336**, 39 (2006).

[20] K. Kusumoto, Jpn J Appl Phys 1 **45**, 7440 (2006).

[21] B. Noheda, D. E. Cox, G. Shirane, S. E. Park, L. E. Cross, and Z. Zhong, Physical Review Letters **86**, 3891 (2001).

[22] D. Vanderbilt and M. Cohen, Physical Review B **63**, 094108 (2001).

[23] Z. G. Ye, B. Noheda, M. Dong, D. Cox, and G. Shirane, Physical Review B **64**, 184114 (2001).

[24] A. Singh and D. Pandey, Physical Review B **67**, 064102 (2003).

[25] C.-S. Tu, I. C. Shih, V. H. Schmidt, and R. Chien, Appl Phys Lett **83**, 1833 (2003).

[26] H. Cao, F. M. Bai, N. G. Wang, J. F. Li, D. Viehland, G. Y. Xu, and G. Shirane, Physical Review B **72**, 064104 (2005).

[27] M. Ahart, et al., Nature **451**, 545 (2008).

[28] C. W. Ahn, C. S. Park, D. Viehland, S. Nahm, D. H. Kang, K. S. Bae, and S. Priya, Japanese Journal of Applied Physics **47**, 8880 (2008).

[29] Y. F. Chang, S. F. Poterala, Z. P. Yang, and G. L. Messing, Journal of the American Ceramic Society, accepted. (2010).

[30] G. L. Messing, et al., Critical Reviews in Solid State and Materials Sciences **29**, 45 (2004).

[31] Y. F. Chang, S. F. Poterala, Z. P. Yang, S. Trolier-McKinstry, and G. L. Messing, Appl Phys Lett **95** (2009).
[32] Y. F. Chang, S. F. Poterala, Z. P. Yang, S. Trolier-McKinstry, and G. L. Messing, J Mater Res **25**, 687 (2010).
[33] R. E. Newnham, *Properties of Materials:Anisotropy, Symmetry, Structure* (Oxford University Press Inc., New York, 2005).
[34] JCPDS-ICDD **#81-2200**.
[35] M. Budimir, D. Damjanovic, and N. Setter, Journal of Applied Physics **94**, 6753 (2003).
[36] D. Damjanovic, Ieee T Ultrason Ferr **56**, 1574 (2009).
[37] H. L. Du, W. C. Zhou, F. Luo, D. M. Zhu, S. B. Qu, and Z. B. Pei, Appl Phys Lett **91** (2007).

Figure captions

FIG. 1. Dielectric, ferroelectric and piezoelectric properties for KNN-2%LN textured ceramics. (a) Dielectric constant ε_r and loss factor tanδ as a function of temperature taken on heating at 1kHz. The inset shows the thermal hysteresis around T_{O-T}; (b) polarization hysteresis loops at various temperatures; (c) unipolar strain vs electric field curves at various temperatures and (d) temperature dependence of high field d_{33}* calculated from the slope of unipolar ε-E curves and remnant polarization P_r.

FIG. 2. Dc-bias dependent dielectric properties for KNN-2%LN textured ceramics. (a) Dielectric constant and (b) dielectric loss factor tanδ as a function of temperature taken on cooling at 1kHz under E_{dc}=0, 2, 4, 6, 8, 10 and 12kV/cm. (c) tunability of ε_r as a function of dc-bias measured at a frequency of 1kHz. (d) T_{O-T} and its hysteresis as a function of dc-bias.

FIG. 3. Dc-bias dependent structural properties for KNN-2%LN textured ceramics. Temperature dependent pseudocubic (200) X-ray linear scans under (a) zero-field and (b) field of 12kV/cm cooled conditions. (c) Temperature dependence of the volume fraction for T and O phase. (d) $(002)_T/[(002)_T+(200)_T]$ and $(022)_O/[(022)_O+(200)_O]$ intensity ratios as a function of temperature under dc bias of E=0, 6 and 12kV/cm.

FIG. 4. Schematics of the possible domain configurations for the T (top row) and O (bottom row) phases under the zero field cooling condition (left column) and field

cooling (right column) conditions. In (a) and (c), white denotes c-domain regions and any gray denotes a-domain ones. On transforming to the O phase, the T c-domains change into its direction four equivalent O domains, which are $[0\bar{1}1]_{cub}$, $[\bar{1}01]_{cub}$, $[011]_{cub}$ and $[101]_{cub}$, as shown in (b) and (d) with thick arrows. The T a-domains change into two equivalent O domains in plane: $[110]_{cub}$ and $[\bar{1}10]_{cub}$, as shown in (b) with thin arrows.

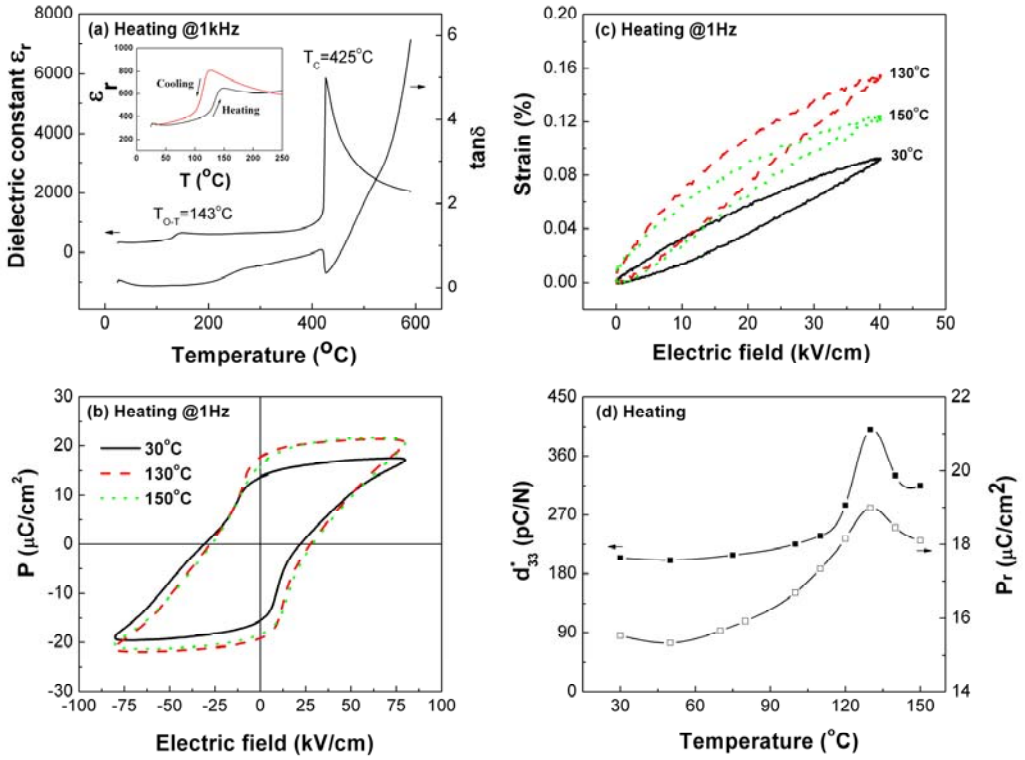
(a) Heating @1kHz
Dielectric constant ε_r
tanδ
T_C=425°C
T_O-T=143°C
Cooling
Heating
T (°C)
Temperature (°C)
(c) Heating @1Hz
Strain (%)
130°C
150°C
30°C
Electric field (kV/cm)
(b) Heating @1Hz
30°C
130°C
150°C
P (μC/cm²)
Electric field (kV/cm)
(d) Heating
d*33 (pC/N)
Pr (μC/cm²)
Temperature (°C)

Figure 1

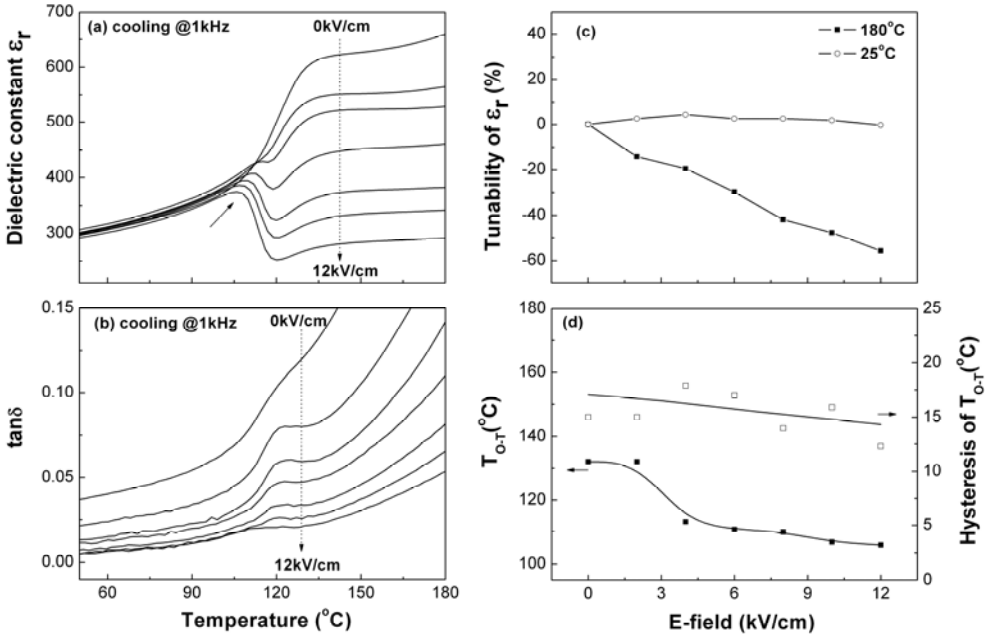
(a) cooling @1kHz
0kV/cm
12kV/cm
Dielectric constant ε_r
(b) cooling @1kHz
0kV/cm
12kV/cm
tanδ
Temperature (°C)
(c)
180°C
25°C
Tunability of ε_r (%)
(d)
T_{o-T}(°C)
Hysteresis of T_{o-T}(°C)
E-field (kV/cm)

Figure 2

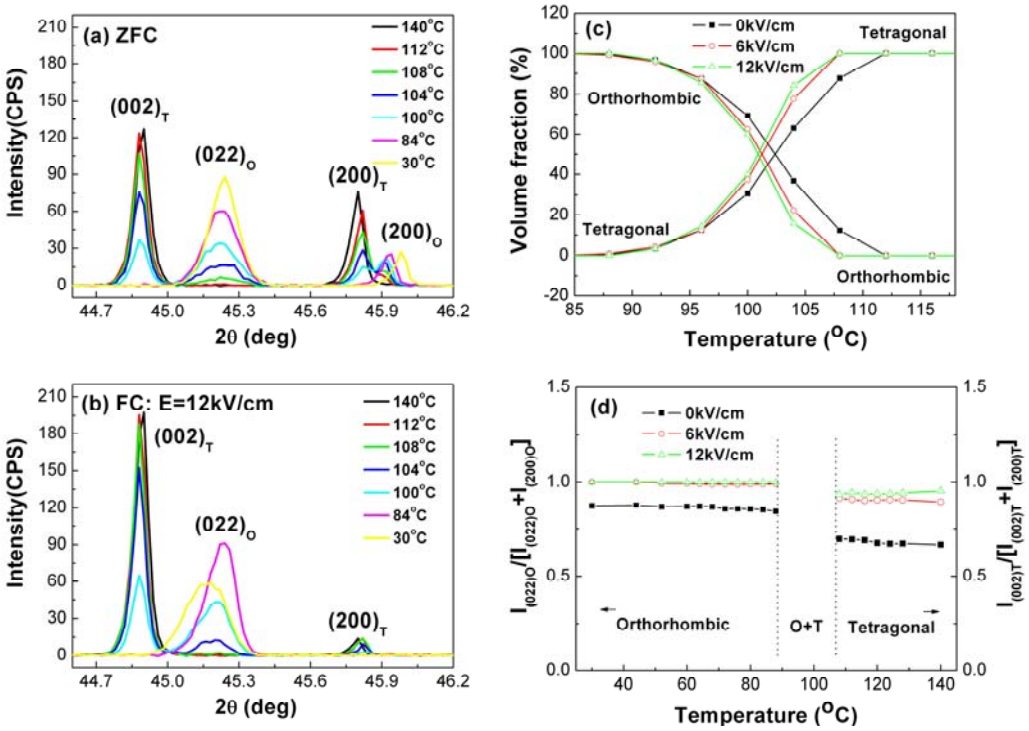
(a) ZFC
140°C
112°C
108°C
104°C
100°C
84°C
30°C
(002)T
(022)O
(200)T
(200)O
Intensity(CPS)
2θ (deg)
(b) FC: E=12kV/cm
(c)
0kV/cm
6kV/cm
12kV/cm
Tetragonal
Orthorhombic
Volume fraction (%)
Temperature (°C)
(d)
O+T
Temperature (°C)

Figure 3

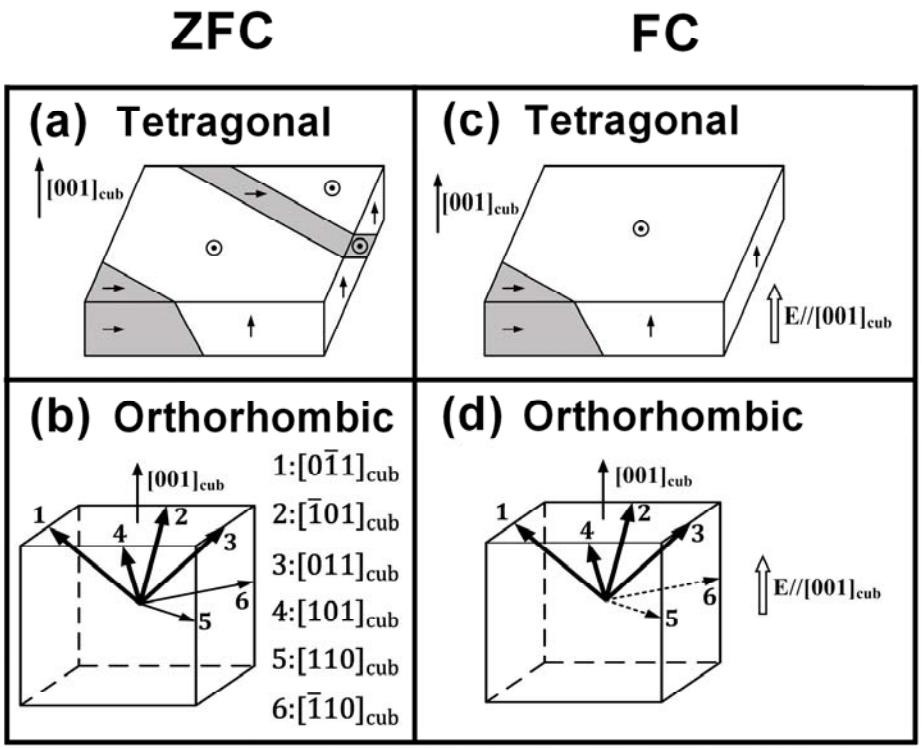
ZFC
FC
(a) Tetragonal
[001]cub
(c) Tetragonal
[001]cub
E//[001]cub
(b) Orthorhombic
[001]cub
1
2
3
4
5
6
1:[0$\bar{1}$1]cub
2:[$\bar{1}$01]cub
3:[011]cub
4:[101]cub
5:[110]cub
6:[$\bar{1}$10]cub
(d) Orthorhombic
[001]cub
E//[001]cub

Figure 4